Dark exoplanets

Yang Bai
Department of Physics, University of Wisconsin-Madison, Madison, Wisconsin 53706, USA

Sida Lu
Institute for Advanced Study, The Hong Kong University of Science and Technology,
Clear Water Bay, Kowloon, Hong Kong, People's Republic of China

Nicholas Orlofsky
Department of Physics, Carleton University, Ottawa, Ontario K1S 5B6, Canada

(Received 29 April 2023; accepted 24 September 2023; published 14 November 2023)

The prevailing assumption is that all exoplanets are made of ordinary matter. However, we propose an unconventional possibility that some exoplanets could be made of dark matter, which we name "dark exoplanets." In this paper, we explore methods to search for dark exoplanets, including the mass-radius relation, spectroscopy, missing transit, and transit light curve. Specifically, we focus on the transit light-curve method and demonstrate how to distinguish partially transparent dark exoplanets from fully opaque ordinary exoplanets using both observed exoplanet data and dark exoplanet mock data. Our analysis shows that dark exoplanets with a large radius (above around 10% of the star radius) and a small optical depth (below around one) can be identified with current telescope sensitivities.

DOI: 10.1103/PhysRevD.108.103026

I. INTRODUCTION

In the last three decades, we have seen tremendous progress on discovering new exoplanets using multiprong detection methods [1]. With ongoing [2–5] and planned future telescopes [6–9], we will not only discover more exoplanets, but also study their properties in great detail. For all existing searches and studies, the exoplanets are assumed to be made of ordinary matter either explicitly or implicitly. On the other hand, there exists another possibility that some exoplanets are made not of ordinary Standard Model (SM) matter, but of dark matter (DM) particles. We explore general search strategies for such "dark exoplanets" in this work.

If DM forms composite states, their masses and/or radii could reach planetary scales or even higher [10–17]. DM models that could form macroscopic states include fermion solitons/Fermi balls [18–21], scalar nontopological solitons/Q-balls [22–30], dark quark nuggets [31–34], dark nuclei [35–39], and mirror sectors or any dark sector with an analog of chemistry or nuclear physics [40,41] or degeneracy pressure [42–45]. Macroscopic DM (MDM) is constrained by microlensing [46–52], among other constraints [15], to be less than $\mathcal{O}(10^{-2})$ of the measured DM energy density for masses greater than about 10^{23} g, and there are prospects to set bounds at still lower masses [53–55]. MDM thus need not make up all of DM, just as stars and planets are only a small fraction of ordinary matter. Interestingly, several excess microlensing events were observed by OGLE that could be interpreted as Earth-mass MDM [56].

A MDM state with its mass and/or radius similar to those of a planet will behave as a dark exoplanet if it is bounded to a star system, even if the object's underlying physics resembles something else entirely. In this work, we remain agnostic about the formation of stellar systems containing dark exoplanets and concentrate on how to search for a dark exoplanet (DEP) and distinguish it from an ordinary exoplanet (OEP).

II. METHODS FOR DETECTING DARK EXOPLANETS ORBITING STARS

We first identify several methods to detect and characterize a DEP orbiting an ordinary star.

(i) *Mass-radius relation:* The masses and radii of some exoplanets can be measured independently, e.g., using radial velocity (RV) or transit timing variation to measure the mass and transit photometry for the radius. An outlier exoplanet with its mass and radius not matching OEP behaviors [57,58] would indicate the presence of a DEP. Some simpler cases of this could happen for a DEP candidate; the inferred planet energy density is even larger than one that is made of only Fe [58], or, an exoplanet with density less than about 0.03 $\mathrm{g/cm^3}$. At present, no such outliers exist. If DEPs do exist, the lack of observational evidence could indicate that they have mass, radius, or weaker interactions with light outside the ability to be probed by present methods, or it could indicate they have size and density very similar to OEPs. It could also indicate that the radius has been mismeasured due to OEP model assumptions (as we will discuss for the case of transits). Alternatively, DEPs orbiting ordinary stars may be rare.

(ii) *Spectroscopy:* During a transit, the spectrum of the sunlight can be measured and compared to the spectrum when the planet is not transiting. Differences may be indicative of absorption in the planet's atmosphere. An absorption spectrum that doesn't match any category of OEP may indicate that the transiting planet is a DEP. In principle, this type of analysis could also extend to the cases of reflection and secondary eclipse. At present there are not very many high-quality spectroscopic measurements of exoplanets, but the James Webb Space Telescope is promising to search for DEPs [59,60].

(iii) *Missing transit:* A combination of RV and astrometry measurements can be used to completely determine the orbital information of an exoplanet [61–70]. If a transit is predicted based on these measurements but not detected, it could indicate the presence of a transparent DEP. In the references here, several exoplanets have the potential for transits, but the inclination angle measurement uncertainties are too large to make definitive predictions.

(iv) *Transit light curve:* Given that transit searches are the most prolific exoplanet finders, and that observations of spectroscopy or RV are currently impractical to perform on every candidate exoplanet, it is interesting to consider whether DEP candidates could be identified using transit searches alone.

Let us elaborate further on the transit light-curve method. For DEPs to be distinctive, we assume they have a suppressed but non-negligible electromagnetic interaction, making the DEPs partially transparent. With the DM particle density n constant and the DM-photon cross section σ energy-independent within the telescope's energy acceptance, this partial transparency is characterized by a transmittance function

$$T(x) = \exp\left(-2\tau_0\sqrt{1-(x/R_p)^2}\right), \quad \text{for } x < R_p, \qquad (1)$$

where x is the distance from the planet's center, R_p is the DEP radius, and $\tau_0 \equiv R_p n \sigma$ denotes the characteristic optical depth. Detailed discussion about MDM models with electrically-charged constituents to have a nonzero τ_0, in analogy to the degenerate Fermi and gravitational pressure balance for the white dwarfs [24,44] is provided in Sec. V.

As a proof of principle, we fit both ordinary and dark exoplanet transit light curves to both real and simulated phase-folded data of exoplanet transits, assuming a one-star–one-planet system with a circular orbit. For simplicity, we take the period T_p as sufficiently well-measured that we do not refit it (for real data, we use published values, and for simulated data we use the known simulated period). The host star's mass M_s and radius R_s are also assumed to be known from independent measurements and modeling, see [1] for a review, and its normalized specific surface intensity is modeled by the quadratic limb darkening formula [71] $I(r)/I(0) = 1 - u_1(1-\sqrt{1-r^2/R_s^2}) - u_2(1-\sqrt{1-r^2/R_s^2})^2$, where r is the distance from the center of the star on the image plane. Hence the semimajor axis of the exoplanet orbit a can be determined. For an OEP, the remaining parameters to fit are the planet radius $r_p \equiv R_p/R_s$, orbital inclination angle i, quadratic limb darkening coefficients u_1 and u_2, and orbital angular position of the first data point on the phase-folded light curve θ_{init} necessary for aligning the transit centers in the model and data (see Appendix A for the orbital geometry including the definition of θ). For a DEP, we must also fit τ_0 so that $T(x)$ in Eq. (1) can be determined. Altogether, we have five and six model parameters for the OEP and DEP models, respectively.

III. DEP SEARCH WITH A CONFIRMED EXOPLANET LIGHT CURVE

Here, we analyze data from a transiting exoplanet, which could serve as an example for examining more transit light curve data. This particular planet was chosen to illustrate how constraining real data can be on the DEP hypothesis, rather than the exoplanet that would be "most likely" to be a DEP, and a full analysis of all the transit data on all known/candidate exoplanets is well beyond the scope of this work. Unsurprisingly, the data analyzed in this section favors the OEP hypothesis over the DEP hypothesis. However, the transit data do not convincingly rule out the DEP hypothesis when taken on their own.

The target exoplanet we use for analysis is K2-44 b [72], which is chosen to demonstrate the Earth-radius planet case in a one-star–one-planet system with a nearly circular orbit (see Appendix B for another example with a Jupiter-radius planet and a similar outcome). We use the pixel level decorrelated, cotrending basis vector (CBV) corrected data provided by the EVEREST 2.0 pipeline [73]. Similar to the treatment in [72], we use the first 3072 epochs out of those with `QUALITY` $= 0$ flag to generate the light curve, and produce the normalized folded light curve through EVEREST with parameters $T_0 =$ 1978.7248 (BJD-2454833), period $= 5.6549$ days, and duration $= 0.3$ days (though see [72] for possible improvements to the data processing).

For this exoplanet, the OEP and DEP best fit parameters and χ^2 values are nearly identical, with the DEP fit favoring $\tau_0 \gg 1$ that is essentially indistinguishable from an OEP. The corresponding light curves are displayed in Fig. 1 (upper panel), in which the best-fit light curves from the

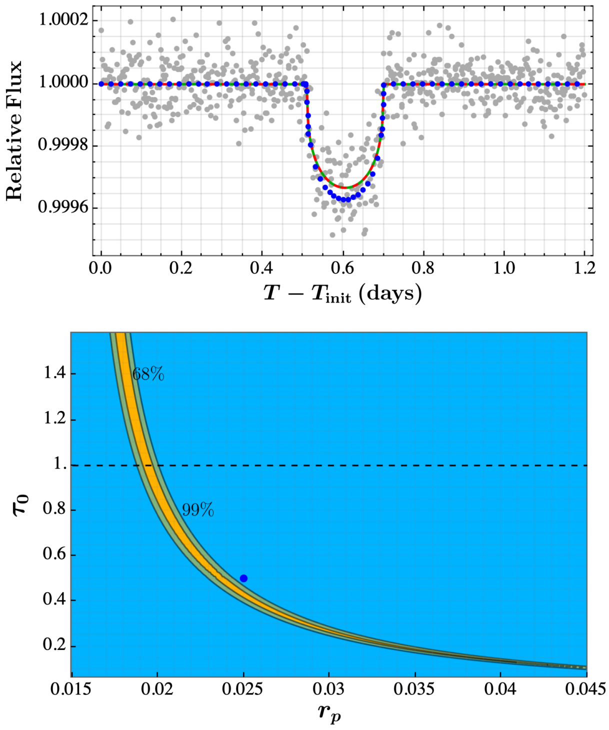

FIG. 1. Top: the measured (normalized and folded) transit light curve of K2-44 b together with light curves from both ordinary and dark exoplanet model fits. T_{init} indicates the time of the leftmost measurement after phase folding the light curves. The solid green and dashed red curves represent the best-fit ordinary and dark exoplanet models, and the dotted blue curve corresponds to the blue dot in the bottom panel. Bottom: contours of $\Delta\chi^2$ from the best-fit point of the DEP model for the K2-44 b measurement. All parameters except r_p and τ_0 are fixed (instead of marginalized) to be the same as the best-fit point. The yellow and green contours differ from the best-fit point at 68% and 99% confidential level for two degrees of freedom.

two models almost completely overlap with each other as expected. The dotted blue curve in the upper panel correspond to the blue dot in the lower panel, which serves as an illustration of deviating from the best-fit region.

On the other hand, while the DEP hypothesis is not favored, it cannot always be excluded. To demonstrate this point, the lower panel of Fig. 1 displays a contour plot of the chi-square goodness of fit on r_p and τ_0, keeping the other parameters fixed to their best-fit values.[1] The two parameters are inversely correlated. At smaller r_p the contours tend to be insensitive to τ_0, as the OEP model can be effectively viewed as a DEP model in the $\tau_0 \to \infty$ limit. At larger r_p the contours of fixed likelihood pinch off, setting a lower bound on τ_0. The 68% confidence bound is $r_p < 0.044$ and $\tau_0 > 0.1$, while the best-fit values are $r_p = 0.0163$ and $\tau_0 = 59$. Note that in the limit of small τ_0 and large radius, the best-fit region follows the relationship $n\sigma \propto r_p^{-3}$ (or $\tau_0 \propto r_p^{-2}$), where two factors of r_p^{-1} come from the cross sectional area of the dark exoplanet and one factor of r_p^{-1} comes from the opacity [where $1 - T(x) \approx 2\tau_0(1 - x^2/R_p^2)^{1/2} + \mathcal{O}(\tau_0^2)$ for small τ_0].

IV. MOCK LIGHT CURVES OF DARK EXOPLANETS

In addition to reexamining the measured transit light curves and searching for DEPs, it is also worthwhile to check whether a mock DEP transit light curve can always be well mimicked by an OEP. Parameter space where the OEP fits fail to explain the data would be the natural target region for DEP hunting.

Mock folded transit light curves are generated in a way such that the host star properties follow the fitted mass-radius relation for ZAMS models [74] and consistent with the host stars of the current observed exoplanets with transit methods. Each mock folded light curve may have 100–250 data points on it, whose error bars are assigned according to the Gaussian distribution $\mathcal{N}(\sigma_e, \Delta\sigma_e)$. We choose $\sigma_e = 10^{-4}$ and $\Delta\sigma_e = 10^{-6}$, consistent with the current measurements from Kepler and TESS [3]. More details on mock data generation are provided in Appendix C. Each mock light curve is fitted with both the DEP and the OEP models, with the corresponding minimal χ^2 denoted as χ^2_{D} and χ^2_{O}, respectively. In addition, we calculate the χ^2_{null} value corresponding to a constant relative flux $\equiv 1$ hypothesis. Letting $F_n(\chi^2)$ be the cumulative distribution function for a chi-square distribution with n degrees of freedom, we identify a mock light curve k with N_k data points as a DEP candidate if (i) $F_{N_k-1}(\chi^2_{\text{null}}) > 0.99$, (ii) $F_{N_k-6-1}(\chi^2_{\text{D}}) < 0.95$, and (iii) $F_{N_k-5-1}(\chi^2_{\text{O}}) > 1 - \alpha$ with $\alpha = 0.01$ or 0.05. The light curves that satisfy (i) but fail (iii) with $\alpha = 5\%$ are identified as OEP candidates, regardless if they satisfy (ii). The rest (not in DEP or OEP categories) are classified as undetectable. Note that the criteria for OEP vs DEP candidates is "conservative" in the sense that if an OEP model provides a good fit, the transiting planet is not classified as a DEP candidate even if the DEP model significantly improves the goodness of fit compared to the OEP.

A total of 1280 sets of mock light curves are generated and examined as above, 120 of which are classified as undetectable. Many of the undetectable light curves correspond to grazing inclination angles i (near their minimum for given a) or small r_p, both of which are harder to detect. The most important parameters distinguishing the DEP from the OEP candidates are r_p and τ_0. As demonstrated in

---

[1] The credible regions are calculated using a χ^2 difference test with two degrees of freedom. In principle, the other parameters could be marginalized to their best-fitting value at each point on this 2D plane, e.g., using a Markov Chain Monte Carlo to sample the posterior distribution. However, the result would not differ much because most of the parameters would still be very close to their best-fit value. The credible regions may be slightly enlarged, but their qualitative features would remain.

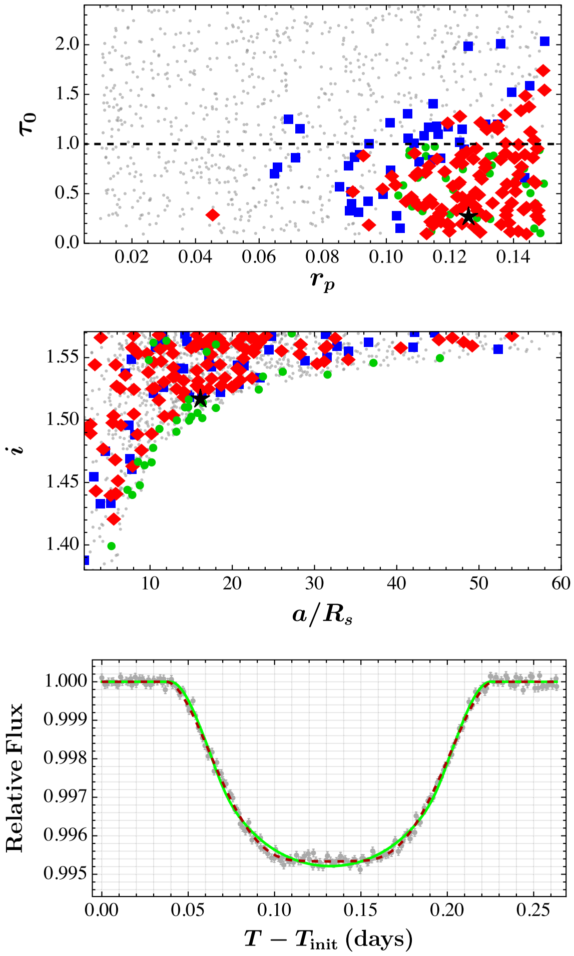

FIG. 2. Top: the scatter plot of all DEP and OEP candidates on the true-value r_p–τ_0 plane. The red diamonds (and black star) are the identified DEP candidates when the OEP model is rejected at $1-\alpha = 99\%$ confidence level, and the blue squares are at $1-\alpha = 95\%$ confidence level. Both the small gray and big green dots are OEP candidates. The green dots are highlighted as they have $r_p > 0.1$ and $\tau_0 < 1$, a similar parameter region to most of the DEP candidates. Mock light curves that are classified as undetectable are not shown. Middle: the same mock data on the true-value a–i plane, with point styles the same as the top panel. Bottom: the best-fitted DEP (dashed red) and OEP (solid green) light curves for the DEP candidate indicated by the black star in the other two panels.

the upper panel of Fig. 2 (for a full corner plot, see Fig. 6), DEPs with large $r_p \gtrsim \mathcal{O}(0.1)$ and small $\tau_0 \lesssim \mathcal{O}(1)$ are the most easily distinguished. This result can be understood in the following way. The DEP light curves distinguish themselves from those of OEPs mainly through the shape of the ingress/egress region, see the bottom panel of Fig. 2 for the fitted light curves in one of the DEP candidates. A larger radius and more transparent (smaller τ_0) DEP has a better chance to manifest such differences.

There are still OEP light curves indistinguishable from DEPs in the region $\tau_0 < 1$ and $r_p > 0.1$, highlighted as green dots in the top and middle panels of Fig. 2. Almost all of them have inclination angles i near their a-dependent minima as shown in the middle panel, meaning that these mock exoplanets just graze the outer edge of their stellar images. Thus, less information is present to distinguish between the stellar limb darkening and DEP opacity effects.

The bottom panel of Fig. 2 shows one example light curve from the mock data where the OEP hypothesis is rejected with $1-\alpha = 99\%$ confidence level but the DEP hypothesis is acceptable. This mock data point is denoted by the black star in the other two panels. The light curves from the best-fitted DEP and OEP models are shown in the dashed-red and green lines, respectively. Note that the best-fit OEP light curve does not show good agreement, particularly near the edges of the ingress and egress regions. The mock data contains 201 data points, and has a true value of $(i, r_p, u_1, u_2, \tau_0, \theta_{\rm init}) = (1.517, 0.126, 0.007, 0.151, 0.274, 4.650)$. The OEP model gives a best fit of $(i, r_p, u_1, u_2, \theta_{\rm init}) = (1.521, 0.073, 0.869, 0.131, 4.650)$. In particular, the OEP model best fit has a much smaller radius r_p than the true value to compensate for its opacity and a bit larger inclination angle i to keep the transit duration fixed with decreasing r_p. The OEP model fit for this light curve also prefers $I(R_s)/I(0) = 1 - u_1 - u_2 \approx 0$, whereas the true value is closer to 0.84. This could be because this particular transit has a somewhat grazing transit with i near its a-dependent minimum (see the middle panel of Fig. 2). Therefore, the small DEP opacity can be partially mimicked by an OEP orbiting a star with dim limbs—either results in a smaller fractional darkening. In fact, as discussed in the Appendix C, it may be easier to distinguish DEPs orbiting stars with larger true values of $I(R_s)/I(0)$, as is the case for this example mock data point.

V. MODEL-DEPENDENT OPACITY OF DARK EXOPLANETS

In the previous sections, the dark exoplanet is modeled to be composed of dark particles with a constant number density n and cross section to interact with light in the wavelengths being observed σ (which may in principle depend on wavelength, especially if the dark sector is complex and contains its own dark chemistry, but which we take as constant here for visible wavelengths measured by transit-hunting telescopes). For instance, dark quark nuggets [33] or nontopological solitons like Q-balls [23] contain either fermion or complex scalar fields as their constituents. Solitons can form from a cosmic phase transition or solitosynthesis, and it has been shown that they can form with radii comparable to planets [29]. Alternatively, a "mirror" dark sector may have particle content approximately matching that of the SM and thus have atomlike states as the building blocks of dark planets (or stars [40,41]). Because mirror particles would behave similarly to SM particles, mirror planets and stars would form from similar formation mechanisms to their SM counterparts, resulting in similar radii and masses. Here, we elaborate further on one DEP model inspired by mirror sectors that can form composite states similar to degenerate compact stars.

Similar to white dwarfs or neutron stars, where the degenerate Fermi pressure balances the gravitational pressure, the dark exoplanet could contain constituent particles with neutral, positively charged, and negatively charged particles with masses m_0, m_+, m_- (see also [11,12,42–45]). Note that m_+ is not necessarily equal to m_-, similar to the unequal mass of electron and proton inside a hydrogen atom. In principle, cosmologically stable and abundant electromagnetically charged dark-sector particles are severely constrained by astronomical and cosmological observations, e.g., the cosmic microwave background [75] and the heating of galactic clouds [76]. These constraints can be relieved if the dark particles are bound into neutral composites by dark interactions before the gravitational interaction becomes important, or if these charged states are only responsible for a fraction of the observed dark matter abundance [77] (see Refs. [78,79] for models with strong dynamics in the dark sector and a neutral composite dark baryon state coupling to photon at higher moments). Alternatively, the heavier charged states may decay into lighter neutral states and charged SM particles in analogy to the neutralino and chargino in supersymmetry (or the neutron and proton if their masses were reversed), and the charged states may only be populated inside of DEPs where the degenerate Fermi energy is sufficiently high and/or there is a deconfined vacuum state where the charged states have smaller masses. Similar to the case of hydrogen where the electron and proton carry individual global symmetries resulting in stable atoms, the annihilations of positively and negatively charged particles are forbidden by some dark flavor symmetries. For simplicity, we assume that the electrically charged particles are much heavier than the neutral particle, $m_+ \approx m_- \gg m_0$, and an equal number density for the three species. Similar to the white dwarf case where the lighter fermion (electron) provides degenerate Fermi pressures while the heavier fermion (proton) provides the main mass, the DEP has the following radius and mass relation

$$\begin{aligned} R_p &\approx \frac{3^{4/3}\pi^{2/3}M_{\rm pl}^2}{8m_0 m_+^{5/3}M_p^{1/3}} \\ &= 1.7R_\oplus \times \left(\frac{10\,\mathrm{keV}}{m_0}\right)\left(\frac{100\,\mathrm{GeV}}{m_+}\right)^{5/3}\left(\frac{M_\oplus}{M_p}\right)^{1/3}, \end{aligned} \tag{2}$$

in the nonrelativistic limit with Fermi momentum $p_F \approx \frac{4}{3^{2/3}\pi^{1/3}} m_0 m_+^{4/3} M_p^{2/3} M_{\rm pl}^{-2}$ and $M_{\rm pl} = 1/\sqrt{G} = 1.22 \times 10^{19}$ GeV. For the nonrelativistic approximation to be valid, $m_+ \ll M_p^{-1/2} M_{\rm pl}^{3/2} = 736\,\mathrm{GeV} \times (M_\oplus/M_p)^{1/2}$. Here, $M_\oplus$ is Earth's mass.

The optical depth is determined by integrating the dark exoplanet density along the line of sight of the light,

$$\begin{aligned} \tau &= \int d\ell (n_+ + n_-)\sigma_{\rm T} \sim 2n_+\sigma_{\rm T}R_p \\ &= \frac{128\alpha^2 m_0^2 m_+^{1/3} M_p^{5/3}}{3^{8/3}\pi^{4/3}M_{\rm pl}^4} \\ &= 1.2 \times 10^{-4} \times \left(\frac{m_0}{10\,\mathrm{keV}}\right)^2 \left(\frac{m_+}{100\,\mathrm{GeV}}\right)^{1/3}\left(\frac{M_p}{M_\oplus}\right)^{5/3}, \end{aligned} \tag{3}$$

where the "Thomson cross section" for photon scattering off a heavy charged particle with $\sigma_{\rm T} = 8\pi\alpha^2/(3m_+^2)$ is used.

For a dark exoplanet model different from a white dwarf, one could have other pressures like the pressures from dark particle self interactions [24] or thermal pressure [44], with or without the vacuum pressure playing a role. The relations of R_p and M_p with charged-particle masses could depend on other model parameters. Therefore, one could still treat R_p and M_p as independent parameters to discuss the opacity of a DEP. If electrically charged particles contribute a sizable fraction to the total DEP mass, the charged-particle number density is $\mathcal{O}[M_p/(2m_+R_p^3)]$ and the optical depth is

$$\begin{aligned} \tau &= \int d\ell (n_+ + n_-)\sigma_{\rm T} \sim 2n_+\sigma_{\rm T}R_p \\ &= \frac{2\alpha^2 M_p}{m_+^3 R_p^2} \\ &= 0.9 \times \left(\frac{10\ \mathrm{GeV}}{m_+}\right)^3 \left(\frac{M_p}{M_{\rm J}}\right)\left(\frac{R_{\rm J}}{R_p}\right)^2, \end{aligned} \tag{4}$$

where $M_{\rm J} = 1.9 \times 10^{27}$ kg and $R_{\rm J} = 7.15 \times 10^7$ m represent Jupiter's mass and radius. Note that the charged particle mass is subject to constraints from collider searches, which require $m_+ \gtrsim 500$ GeV [80] in the normal vacuum. On the other hand, if charged particles inside the DEP are not in a normal vacuum state, their masses could be different. For instance, if the charged particles in the normal vacuum are some dark baryon state from a dark QCD-like confining gauge interaction, their charged constituent (dark quark) masses could be smaller in the deconfined vacuum state of the DEP, similar in spirit to Refs. [15,44].

The fraction of star light blocked by a DEP fully occulting its host star is estimated by accounting for the ratio of the cross-sectional areas of the DEP and host star

$$\frac{\Phi_{\text{blocked}}}{\Phi_0} \sim \frac{R_p^2}{R_s^2}\tau = \frac{2\alpha^2 M_p}{m_+^3 R_s^2} = 0.009 \times \left(\frac{10\ \text{GeV}}{m_+}\right)^3 \left(\frac{M_p}{M_{\text{J}}}\right)\left(\frac{R_\odot}{R_s}\right)^2. \quad (5)$$

Here, we used the optical depth for the generalized model in (4). We have checked that some other operators coupling DEP particles to the photon—such as the scalar charge radius operator, scalar Rayleigh operator, and fermion magnetic dipole operator—give $\Phi_{\text{blocked}}/\Phi_0$ too small to be detectable as discussed in Appendix D.

Another effect that could impact the opacity is the capture of SM matter by the DEP. Captured SM matter may be expected to quickly thermalize with the DEP and sink to the planet's core, in analogy with stellar capture of DM. This may lead to a core that is more opaque than it would be if the DEP is only made of DM, as has been assumed in the calculations above. Thus, the planet may have an opaque core surrounded by a semitransparent "mantle." We neglect this possibility in this work, but it may be worthy of future study. The captured SM matter could also lead to optical emission signals, as studied in [40,41,81] for the case of dark stars.

VI. DISCUSSION

In this work, we discuss several approaches for the discovery and identification of DEPs. In particular, the DEP transit light curve may not be well-mimicked by an OEP when the DEP is relatively transparent and has a large radius. On the other hand, smaller-radius or larger-opacity DEPs could be hiding in existing transit data masquerading as OEPs.

There are several possible improvements to our work. For simplicity we considered only circular orbits for both the dark and ordinary exoplanets. Additionally, we do not account for the secondary eclipse of the planet passing behind the star, which may reveal more about the exoplanet properties and help distinguish DEPs from OEPs. Other properties we neglect include planetary rings, moons, oblateness, atmospheric or topographic features, night-side emission, star spots, stellar rotation, and gravitational darkening, among others. It is possible that these effects may be confused for opacity effects in a full data analysis.

To see a transiting DEP, it must become gravitationally bound to an ordinary star. If stars tend to be born in regions of enhanced dark matter density (in analogy to early stars [82], though it is unclear if this is true for later-forming stars), then the DEP may become bound *in situ*. Alternatively, the DEP may be captured in a similar way to free-floating planets. While it has been argued (including in the context of Planet Nine [83,84], which could itself very speculatively be a DEP) that capture of free-floating planets is rare [85–91], it is no less likely for a free-floating DEP to be captured than a free-floating OEP of a similar mass [92]. Another possibility is if a free-floating DEP passes through a star, its interactions with the star could slow it enough to allow it to become bound. Further study on early DEP-stellar-system formation and DEP capture would help in elucidating the possibility of detecting DEPs and would be necessary for bounds to be set on DEP abundance if they are not detected.

ACKNOWLEDGMENTS

The authors thank Daniel del Ser and Leo W. H. Fung for useful discussions. This research has made use of the NASA Exoplanet Archive, which is operated by the California Institute of Technology, under contract with the National Aeronautics and Space Administration under the Exoplanet Exploration Program. The work of Y. B. is supported by the U.S. Department of Energy under Contract No. DE-SC-0017647. The work of S. L. is supported by the Area of Excellence (AoE) under the Grant No. AoE/P-404/18-3 issued by the Research Grants Council of Hong Kong S. A. R. The work of N. O. is supported by the Arthur B. McDonald Canadian Astroparticle Physics Research Institute.

APPENDIX A: TRANSIT LIGHT CURVE FOR PARTIALLY TRANSPARENT EXOPLANETS

Because DM must have a suppressed interaction with the photon, an exoplanet made of DM may not be completely opaque. A DEP transit light curve will be affected as a result, and in particularly the reduction in flux should be smaller than that from a same-radius OEP. Here we present the calculation of the transit light curve of a DEP in a model-independent way.

We assume a quadratic stellar limb darkening as in the main text. The unblocked total "flux" from the star is then $\Phi_0 \equiv 2\pi \int_0^{R_s} r dr I(r)/I(0) = \pi R_s^2(6 - 2u_1 - u_2)/6$, where the unit mismatch comes from the normalization factor.

When the exoplanet blocks the star light—i.e., when the distance d between the star and planet's centers projected on the image plane satisfies $d < R_s + R_p$—the blocked flux is

$$\Phi_{\text{blocked}} = \int_0^{R_p} x dx 2[1 - T(x)] \times \int_0^{\phi_0} d\phi \frac{I(\sqrt{x^2 + d^2 - 2xd\cos\phi})}{I(0)}, \quad (\text{A1})$$

where the definition of the quantities are given in Figs. 3 and 4. With the quadratic surface intensity from the main text, for an OEP this integration has an analytic result [93] due to the complete opaqueness of the exoplanet. For a DEP, only the inner angular integration can be done analytically, i.e.,

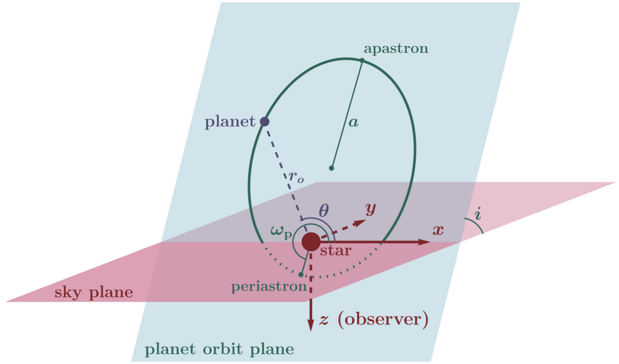

FIG. 3. An illustration for the geometry of an orbiting planet. Here, a is the semimajor axis, i is the inclination angle, ω_p is the argument of periapsis, and r_o is the distance between the planet and star centers.

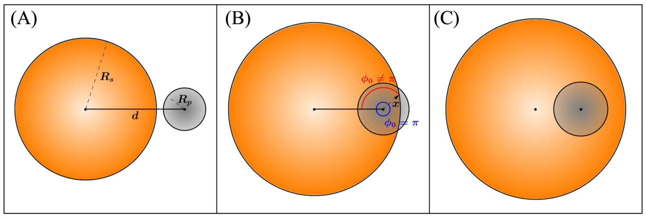

FIG. 4. Some possible relative relationships between the stellar image and the DEP image. In panel (A), the two images are not in contact with each other. In panel (B), the DEP image partially enters the stellar image, corresponding to the ingress or egress region of the light curve. In this situation, the upper limit of the angular integral differs for different x, as shown in Eq. (A3). In panel (C), the DEP image enters the stellar image completely.

$$\begin{aligned}
&\int_0^{\phi_0} d\phi \frac{I(\sqrt{x^2+d^2-2xd\cos\phi})}{I(0)} \\
&= \frac{1}{R_s^2}\Bigg[(u_2(d^2+x^2)+(1-u_1-2u_2)R_s^2)\phi_0 \\
&\quad - 2u_2 dx \sin\phi_0 + 2(u_1+2u_2)R_s\sqrt{R_s^2-(d-x)^2} \\
&\quad \times E\left(\frac{\phi_0}{2}, \frac{4dx}{R_s^2-(d-x)^2}\right)\Bigg],
\end{aligned} \tag{A2}$$

where $E(\varphi, m) = \int_0^\varphi d\phi (1 - m\sin^2\phi)^{1/2}$ is the elliptical integral of the second kind.[2] Depending on the relative location between the stellar image and the dark exoplanet image, the angular integration upper limit is given by

$$\phi_0 = \begin{cases} \arccos\left(\frac{x^2+d^2-R_s^2}{2xd}\right), & x > R_s - d, \\ \pi, & x \leq R_s - d. \end{cases} \tag{A3}$$

The normalized light curve is then calculated by $(\Phi_0 - \Phi_\mathrm{blocked})/\Phi_0$.

APPENDIX B: MORE DETAILS ON THE CONFIRMED EXOPLANET FITS

Here, we give details of the analysis of an additional confirmed exoplanet CoRoT-1 b and show the best fit results for both CoRoT-1 b and K2-44 b in the main text. CoRoT-1 b was chosen because it has a larger Jupiter-sized radius to compare to the Earth-radius of K2-44 b. For CoRoT-1 b, we use the processed light curve data from the VLT observatory in [95]. Otherwise, the methods are the same as K2-44 b in the main text.

The best fit parameters for the OEP and DEP light curve fits of CoRoT-1 b and K2-44 b are given in Table I. For both, the OEP model is statistically favored over the DEP, and the DEP model gives such a large τ_0 that it is practically indistinguishable from the OEP model anyways.

In Fig. 5, we display the light curve and region of preferred r_p and τ_0 in analogy with Fig. 1. The 68% confidence bound for CoRoT-1 b is $r_p < 0.149$ and $\tau_0 > 1.6$. The τ_0 bound is stronger for CoRoT-1 b than for K2-44 b, which can be attributed to CoRoT-1 b's larger radius.

It may be noted that while we have conservatively allowed the values of the limb darkening parameters to float to their best-fit points (subject to physical constraints

TABLE I. The best-fit parameters of CoRoT-1 b and K2-44 b for both OEP and DEP models. The orbits are assumed to be circular for simplicity. The orbital radii and periods are fixed to be the same values as the accepted ordinary exoplanet measurements [72,96], as the period is very well-measured. The orbital inclination i, initial phase of the folded light curve θ_init, limb darkening coefficients (u_1, u_2), and exoplanet radius $r_p \equiv R_p/R_s$ are fitted in both cases, while the dark exoplanet case has an additional fitted parameter of the optical depth τ_0.

	CoRoT-1 b		K2-44 b	
$a(R_s)$	4.910		8.760	
T_p (days)	1.509		5.655	
	OEP	DEP	OEP	DEP
i (rad)	1.486	1.486	1.525	1.525
θ_init (rad)	4.433	4.433	4.041	4.041
u_1	0	0	0.618	0.619
u_2	0.705	0.705	0.228	0.227
r_p	0.136	0.137	0.0163	0.0163
τ_0		81.46		59.23
χ^2	127.97	127.95	858.10	858.09
Degrees of freedom	97	96	659	658

---

[2] Numerically, it is more efficient to use Carlson elliptic integrals [94] in place of the ordinary elliptic integral using the identity $E(\varphi, m) = \sin\varphi R_F(\cos^2\varphi, 1 - m\sin^2\varphi, 1) - \frac{1}{3} m \sin^3\varphi R_D(\cos^2\varphi, 1 - m\sin^2\varphi, 1)$ with the two functions R_F and R_D defined in Ref. [94].

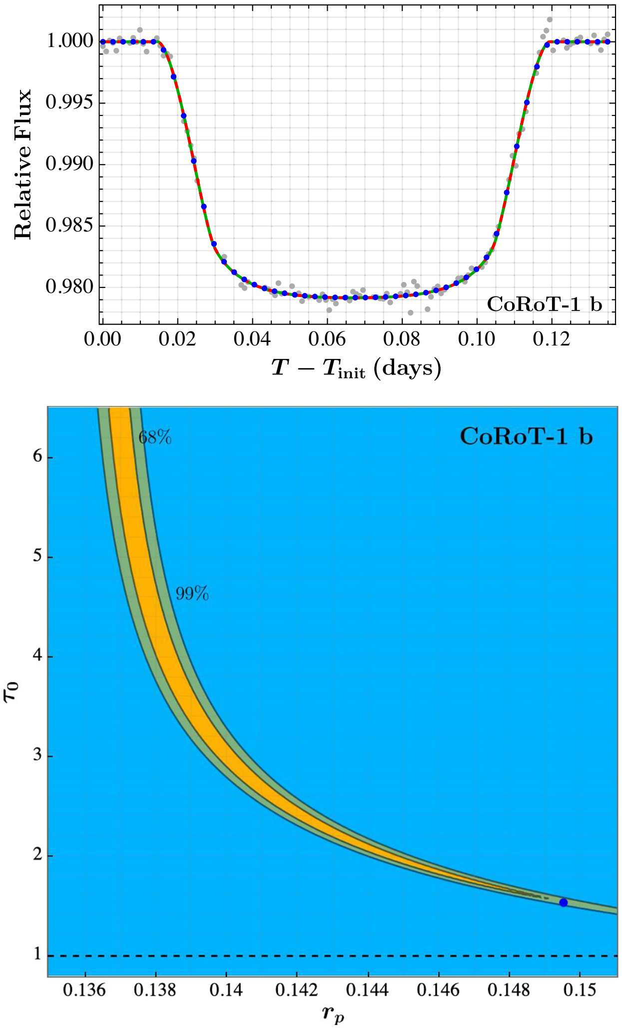

FIG. 5. Same as Fig. 1, but for CoRoT-1 b.

on the brightness being monotonically decreasing from the center and nonnegative), there has been work on classifying the limb darkening parameters based on other stellar properties [97]. If we impose these empirical constraints as priors on our fits, they may change the results on a case-by-case basis.

APPENDIX C: MORE DETAILS ON THE MOCK DATA ANALYSIS

In this section, we provide the details of mock data generation and additional analysis of the mock data presented in Fig. 2.

The mock data are generated in the following way. The mass of the host star M_s is uniformly chosen from 0.5–$5M_{\odot}$, where $_{\odot}$ represents the Sun (note that $\gtrsim 90\%$ of the exoplanets confirmed with the transit method have their host star heavier than $0.5M_{\odot}$). The stellar radius is determined as $R_s = e^g R(M_s)$, with

$$\frac{R(M_s)}{R_{\odot}} = \begin{cases} 0.89(M_s/M_{\odot})^{0.89}, & M_s \leqslant 1.66 M_{\odot}, \\ 1.01(M_s/M_{\odot})^{0.57}, & M_s > 1.66 M_{\odot}, \end{cases} \tag{C1}$$

which is the fitted mass-radius relation for ZAMS models [74], and g a random variable from a normal distribution $\mathcal{N}(\mu = 0, \sigma = 0.5)$ responsible for the deviation from this relation.[3] The orbit of the DEP is assumed to be circular, and the period is uniformly chosen from 1–20 days, a region where ∼75% of the current measured transit events lie (due in part to observational bias). The semimajor axis a is then determined with the Kepler's third law, and we require $a/R_s > 2$. The limb darkening coefficients u_1 and u_2 are uniformly chosen on the region $u_1 > 0, u_1 + u_2 < 1$ and $u_1 + 2u_2 > 0$, which enforces that $I(r)$ is monotonically decreasing and nonnegative. The radius of the DEP is uniformly chosen from $r_p \in [0.01, 0.15]$, and the orbital plane inclination angle i is uniformly chosen between $\arccos[(R_p + R_s)/a]$ (such that there will be a transit event) and $\pi/2$. The optical depth parameter is chosen uniformly from $\tau_0 \in [0.1, 3]$. Each simulated light curve is chosen to cover an orbital angular position $\theta \in [(1.5 - 0.01 n_t)\pi, (1.5 + 0.01 n_t)\pi]$, where n_t is the minimal integer such that $\theta = (1.5 - 0.01 n_t)\pi$ is earlier than the corresponding DEP's ingress (note that for a circular orbit the transit is symmetric around $\theta = 1.5\pi$). This angular position region in θ is evenly divided into N segments, where N is randomly uniformly chosen on [100, 250], and on each segment an angular position is chosen randomly and uniformly, as the light curve used for fitting is phase folded. The error bar size of data point j is set to be $e_j = \sigma_e + \mathcal{N}(0, \Delta\sigma_e)$, where we choose $\sigma_e = 10^{-4}$ and $\Delta\sigma_e = 10^{-6}$, values comparable to the error bar sizes and fluctuations of the current measurements from Kepler and TESS [3]. The center value of this data point is then set to be its model value plus a random number from $\mathcal{N}(0, e_j)$.

A full corner plot of the mock DEP data parameters, with those points that can statistically distinguish between DEPs and OEPs, is shown in Fig. 6. Note that the top and middle panels of Fig. 2 are contained within this plot (except the green circles of Fig. 2 are simply shown as gray circles here).

In addition to the DEP candidate preferences on r_p, τ_0, and i noted in the main text, there is also in Fig. 6 a preference compared to the OEP candidates for the DEP

---

[3] Actually, the stellar radii for confirmed exoplanets are slightly larger than the ZAMS model, likely due to selection bias [98,99], but the effect is small enough that we neglect it here. We focus here on main sequence stars because almost all exoplanets discovered using the transit method orbit main sequence stars [1]. While only a few exoplanets are known around white dwarfs [100], transits of smaller objects like minor planets (radius $\lesssim 1000$ km) are easier to discern in white dwarf systems, which could make them interesting candidates for future study of smaller DEPs.

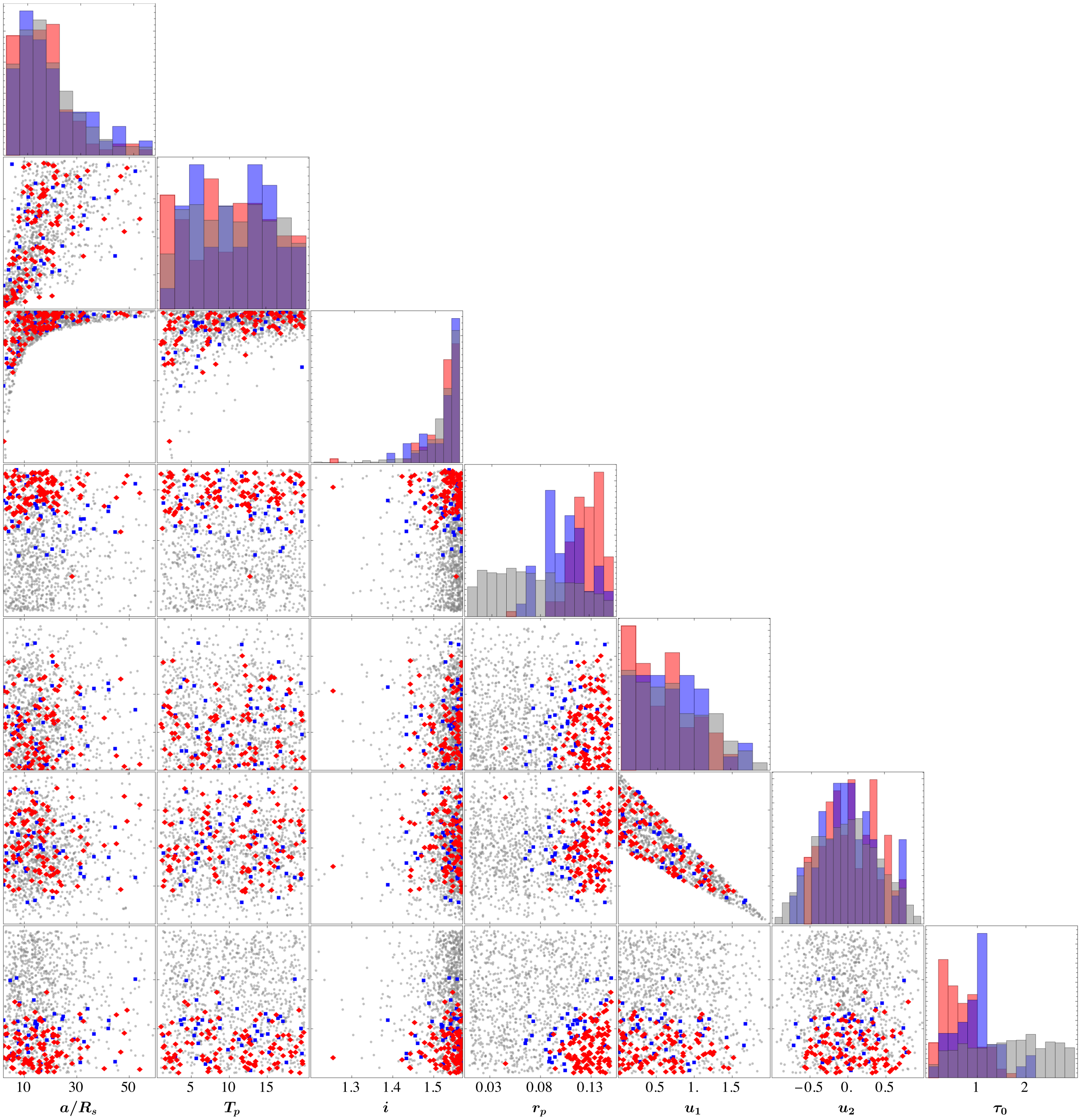

FIG. 6. The full corner plot for the DEP and OEP candidates based on DEP mock data, grouped with parameters among $(a, T_p, i, r_p, u_1, u_2, \tau_0)$. The point styles and selection criteria are the same as those in Fig. 2, except with the green dots remaining gray here. The top panel of Fig. 2 can be found in the bottom row, fourth column, and the middle panel of Fig. 2 is in the third row, first column.

candidates to have u_2 not too close to its maximum or minimum ±1. For such values, $I(R_s)/I(0) = 1 - u_1 - u_2$ is close to zero, so it may be easier to confuse limb darkening and DEP opacity effects for such stars. Indeed, the histogram in Fig. 7 for the $I(R_s)/I(0)$ distribution shows a preference for larger values of this parameter in the DEP candidates compared to the OEP candidates, indicating a preference for stars that are more uniformly bright.

Figure 8 shows a plot of the fractional difference between the fitted and generated DEP parameters for r_p and τ_0. Note that the parameters r_p and τ_0 are inversely correlated in their errors. Intuitively, when τ_0 is overestimated, r_p tends to be underestimated and vice versa

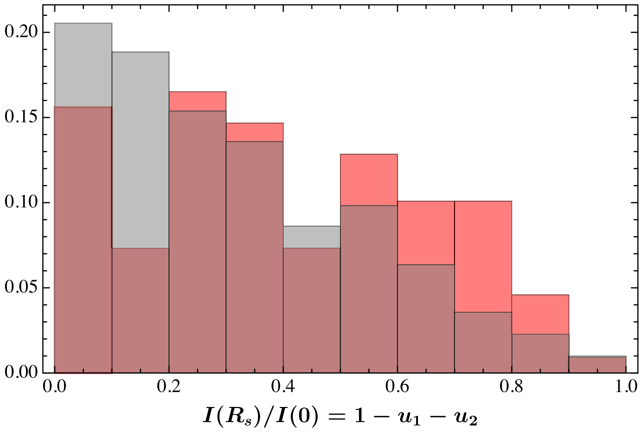

FIG. 7. The probability distribution of $I(R_s)/I(0) = 1 - u_1 - u_2$ for the DEP $\alpha = 0.01$ (red) and OEP (gray) candidate mock data. The DEP $0.01 < \alpha < 0.05$ candidates (blue points in previous figures) are not plotted for easier readability.

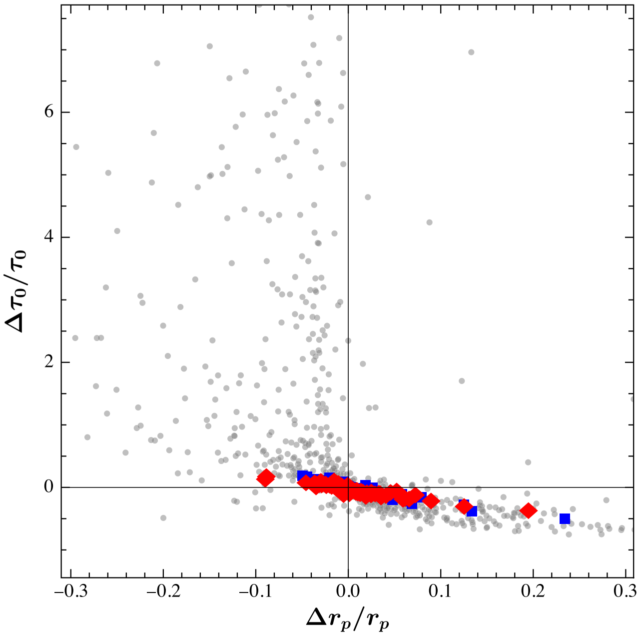

FIG. 8. Plot for the mock data presented in Fig. 6 showing the fractional difference between the generated and fitted DEP parameters. Positive (negative) values indicate the fitted value is greater (smaller) than the generated "true" value.

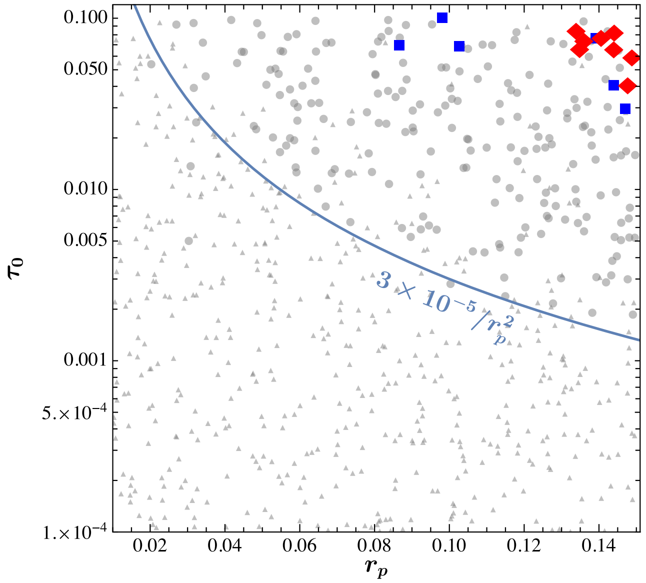

FIG. 9. Similar to the top panel of Fig. 2, but with another set of mock data focusing on small $\tau_0 < 10^{-1}$. Light brown triangles indicate mock DEPs that are classified as undetectable. The gray circle points are selected as OEP candidates. All other point styles are the same as Fig. 2. The blue line indicates $r_p^2\tau_0 = 3\times10^{-5}$.

because the fractional dimming of the star must be held constant. Indeed, as explained in the main text, when $\tau_0 < 1$, the best-fitting regions obey $\tau_0 \propto r_p^{-2}$. For the gray points, when $\tau_0 \gg 1$ the points are essentially degenerate in τ_0, so some points can have large fractional differences for their best-fit points (some of these are cut off by the plot range).

APPENDIX D: SMALL OPACITY LIMIT

To investigate how transparent a DEP can be before it is undetectable, we simulate another 1000 mock DEP light curves sampling logarithmically in $\tau_0 \in [10^{-5}, 10^{-1}]$ but with all other sampling criteria the same as before. The fitted results are plotted in Fig. 9 in analogy to the top panel of Fig. 2. All of the OEP candidate points are shown in gray circle points here. The light brown triangles indicate those where the DEP mock light curves are classified as undetectable, i.e., indistinguishable from a flat light curve. We expected that points with $r_p^2\tau_0 \lesssim \sigma_e/\sqrt{N_{\rm data}} \sim 10^{-5}$ would be undetectable, and indeed the boundary between detectable and undetectable exoplanets are roughly described by the blue curve of $r_p^2\tau_0 = 3\times10^{-5}$, where the factor 3 is chosen manually. However, a much larger $r_p^2\tau_0$ than this is necessary to differentiate between OEPs and DEPs. Specifically, the DEP candidates satisfy $r_p \gtrsim 0.1$ (as before) and $\tau_0 \gtrsim 0.05$. This is because for too small $r_p^2\tau_0$, the reduction in flux in the transit light curve is too shallow to distinguish the two models.

[1] M. Perryman, *The Exoplanet Handbook*, 2nd ed. (Cambridge University Press, Cambridge, England, 2018), 10.1017/9781108304160.

[2] M. Perryman, J. Hartman, G. Á. Bakos, and L. Lindegren, Astrophys. J. **797**, 14 (2014).

[3] G. R. Ricker *et al.*, J. Astron. Telesc. Instrum. Syst. **1**, 014003 (2015).

[4] W. Benz *et al.*, Exp. Astron. **51**, 109 (2021).

[5] J. P. Gardner *et al.*, Space Sci. Rev. **123**, 485 (2006).

[6] H. Rauer *et al.*, Exp. Astron. **38**, 249 (2014).

[7] G. Tinetti *et al.* arXiv:2104.04824.

[8] D. Spergel *et al.* arXiv:1503.03757.

[9] P. Tuthill, E. Bendek, O. Guyon, A. Horton, B. Jeffries, N. Jovanovic, P. Klupar, K. Larkin, B. Norris, B. Pope, and M. Shao, in *Optical and Infrared Interferometry and Imaging VI*, Society of Photo-Optical Instrumentation Engineers (SPIE) Conference Series Vol. 10701, edited by M. J. Creech-Eakman, P. G. Tuthill, and A. Mérand (SPIE, Bellingham, Washington, 2018), p. 107011J.

[10] D. M. Jacobs, G. D. Starkman, and B. W. Lynn, Mon. Not. R. Astron. Soc. **450**, 3418 (2015).

[11] C. Kouvaris and N. G. Nielsen, Phys. Rev. D **92**, 063526 (2015).

[12] G. F. Giudice, M. McCullough, and A. Urbano, J. Cosmol. Astropart. Phys. 10 (2016) 001.

[13] J. A. Dror, H. Ramani, T. Trickle, and K. M. Zurek, Phys. Rev. D **100**, 023003 (2019).

[14] D. Croon, D. McKeen, and N. Raj, Phys. Rev. D **101**, 083013 (2020).

[15] Y. Bai, A. J. Long, and S. Lu, J. Cosmol. Astropart. Phys. 09 (2020) 044.

[16] A. Bhoonah, J. Bramante, S. Schon, and N. Song, Phys. Rev. D **103**, 123026 (2021).

[17] P. Dhakal, S. Prohira, C. V. Cappiello, J. F. Beacom, S. Palo, and J. Marino, Phys. Rev. D **107**, 043026 (2023).

[18] T. D. Lee and Y. Pang, Phys. Rev. D **35**, 3678 (1987).

[19] A. L. Macpherson and B. A. Campbell, Phys. Lett. B **347**, 205 (1995).

[20] J.-P. Hong, S. Jung, and K.-P. Xie, Phys. Rev. D **102**, 075028 (2020).

[21] L. Del Grosso, G. Franciolini, P. Pani, and A. Urbano, Phys. Rev. D **108**, 044024 (2023).

[22] R. Friedberg, T. D. Lee, and A. Sirlin, Phys. Rev. D **13**, 2739 (1976).

[23] S. R. Coleman, Nucl. Phys. **B262**, 263 (1985); **B269**, 744 (A) (1986).

[24] T. D. Lee and Y. Pang, Phys. Rep. **221**, 251 (1992).

[25] E. Pontón, Y. Bai, and B. Jain, J. High Energy Phys. 09 (2019) 011.

[26] E. Y. Nugaev and A. V. Shkerin, J. Exp. Theor. Phys. **130**, 301 (2020).

[27] J. Heeck, A. Rajaraman, R. Riley, and C. B. Verhaaren, Phys. Rev. D **103**, 045008 (2021).

[28] Y. Bai, S. Lu, and N. Orlofsky, J. High Energy Phys. 01 (2022) 109.

[29] Y. Bai, S. Lu, and N. Orlofsky, J. High Energy Phys. 10 (2022) 181.

[30] A. Ansari, L. Singh Bhandari, and A. M. Thalapillil, arXiv:2302.11590.

[31] G. Krnjaic and K. Sigurdson, Phys. Lett. B **751**, 464 (2015).

[32] Y. Bai and A. J. Long, J. High Energy Phys. 06 (2018) 072.

[33] Y. Bai, A. J. Long, and S. Lu, Phys. Rev. D **99**, 055047 (2019).

[34] X. Liang and A. Zhitnitsky, Phys. Rev. D **94**, 083502 (2016).

[35] M. B. Wise and Y. Zhang, Phys. Rev. D **90**, 055030 (2014); **91**, 039907(E) (2015).

[36] M. B. Wise and Y. Zhang, J. High Energy Phys. 02 (2015) 023; 10 (2015) 165(E).

[37] E. Hardy, R. Lasenby, J. March-Russell, and S. M. West, J. High Energy Phys. 06 (2015) 011.

[38] M. I. Gresham, H. K. Lou, and K. M. Zurek, Phys. Rev. D **96**, 096012 (2017).

[39] M. I. Gresham, H. K. Lou, and K. M. Zurek, Phys. Rev. D **97**, 036003 (2018).

[40] D. Curtin and J. Setford, Phys. Lett. B **804**, 135391 (2020).

[41] D. Curtin and J. Setford, J. High Energy Phys. 03 (2020) 041.

[42] A. Maselli, P. Pnigouras, N. G. Nielsen, C. Kouvaris, and K. D. Kokkotas, Phys. Rev. D **96**, 023005 (2017).

[43] M. Hippert, J. Setford, H. Tan, D. Curtin, J. Noronha-Hostler, and N. Yunes, Phys. Rev. D **106**, 035025 (2022).

[44] C. Gross, G. Landini, A. Strumia, and D. Teresi, J. High Energy Phys. 09 (2021) 033.

[45] M. Ryan and D. Radice, Phys. Rev. D **105**, 115034 (2022).

[46] H. Niikura *et al.*, Nat. Astron. **3**, 524 (2019).

[47] N. Smyth, S. Profumo, S. English, T. Jeltema, K. McKinnon, and P. Guhathakurta, Phys. Rev. D **101**, 063005 (2020).

[48] R. A. Allsman *et al.* (Macho Collaboration), Astrophys. J. Lett. **550**, L169 (2001).

[49] P. Tisserand *et al.* (EROS-2 Collaboration), Astron. Astrophys. **469**, 387 (2007).

[50] L. Wyrzykowski *et al.*, Mon. Not. R. Astron. Soc. **416**, 2949 (2011).

[51] K. Griest, A. M. Cieplak, and M. J. Lehner, Astrophys. J. **786**, 158 (2014).

[52] M. Oguri, J. M. Diego, N. Kaiser, P. L. Kelly, and T. Broadhurst, Phys. Rev. D **97**, 023518 (2018).

[53] A. Katz, J. Kopp, S. Sibiryakov, and W. Xue, J. Cosmol. Astropart. Phys. 12 (2018) 005.

[54] Y. Bai and N. Orlofsky, Phys. Rev. D **99**, 123019 (2019).

[55] S. Jung and T. Kim, Phys. Rev. Res. **2**, 013113 (2020).

[56] H. Niikura, M. Takada, S. Yokoyama, T. Sumi, and S. Masaki, Phys. Rev. D **99**, 083503 (2019).

[57] L. Zeng *et al.*, Proc. Natl. Acad. Sci. U.S.A. **116**, 9723 (2019).

[58] S. Seager, M. Kuchner, C. A. Hier-Majumder, and B. Militzer, Astrophys. J. **669**, 1279 (2007).

[59] The JWST Transiting Exoplanet Community Early Release Science Team, arXiv:2208.11692.

[60] S.-M. Tsai *et al.*, arXiv:2211.10490.

[61] B. E. McArthur, G. F. Benedict, G. W. Henry, A. Hatzes, W. D. Cochran, T. E. Harrison, C. Johns-Krull, and E. Nelan, Astrophys. J. **795**, 41 (2014).

[62] J. Rey *et al.*, Astron. Astrophys. **601**, A9 (2017).

[63] F. Feng, G. Anglada-Escudé, M. Tuomi, H. R. A. Jones, J. Chanamé, P. R. Butler, and M. Janson, Mon. Not. R. Astron. Soc. **490**, 5002 (2019).

[64] F. Feng, R. P. Butler, H. R. A. Jones, M. W. Phillips, S. S. Vogt, R. Oppenheimer, B. Holden, J. Burt, and A. P. Boss, Mon. Not. R. Astron. Soc. **507**, 2856 (2021).

[65] J. Llop-Sayson *et al.*, Astron. J. **162**, 181 (2021).

[66] Y. Li, T. D. Brandt, G. M. Brandt, T. J. Dupuy, D. Michalik, R. Jensen-Clem, Y. Zeng, J. Faherty, and E. L. Mitra, Astron. J. **162**, 266 (2021).

[67] S. Hinkley *et al.*, arXiv:2208.04867.

[68] F. Feng *et al.*, Astrophys. J. Suppl. Ser. **262**, 21 (2022).

[69] J. N. Winn, Astron. J. **164**, 196 (2022).

[70] A. Sozzetti, P. Giacobbe, M. G. Lattanzi, and M. Pinamonti, Mon. Not. R. Astron. Soc. **520**, 1748 (2023).

[71] D. M. Kipping, Mon. Not. R. Astron. Soc. **435**, 2152 (2013).

[72] D. del Ser and O. Fors, Mon. Not. R. Astron. Soc. **498**, 2778 (2020).

[73] R. Luger, E. Kruse, D. Foreman-Mackey, E. Agol, and N. Saunders, Astron. J. **156**, 99 (2018).

[74] O. Demircan and G. Kahraman, Astrophys. Space Sci. **181**, 313 (1991).

[75] V. Gluscevic and K. K. Boddy, Phys. Rev. Lett. **121**, 081301 (2018).

[76] A. Bhoonah, J. Bramante, F. Elahi, and S. Schon, Phys. Rev. Lett. **121**, 131101 (2018).

[77] A. Berlin, D. Hooper, G. Krnjaic, and S. D. McDermott, Phys. Rev. Lett. **121**, 011102 (2018).

[78] T. Appelquist *et al.*, Phys. Rev. Lett. **115**, 171803 (2015).

[79] G. D. Kribs and E. T. Neil, Int. J. Mod. Phys. A **31**, 1643004 (2016).

[80] S. Chatrchyan *et al.* (CMS Collaboration), J. High Energy Phys. 07 (2013) 122; 11 (2022) 149(E).

[81] B. B. Kamenetskaia, A. Brenner, A. Ibarra, and C. Kouvaris, arXiv:2211.05845.

[82] T. Abel, G. L. Bryan, and M. L. Norman, Science **295**, 93 (2002).

[83] K. Batygin and M. E. Brown, Astron. J. **151**, 22 (2016).

[84] K. Batygin, F. C. Adams, M. E. Brown, and J. C. Becker, Phys. Rep. **805**, 1 (2019).

[85] A. Gould, Astrophys. J. **368**, 610 (1991).

[86] A. H. G. Peter, Phys. Rev. D **79**, 103533 (2009).

[87] G. Li and F. C. Adams, Astrophys. J. **823**, L3 (2016).

[88] A. J. Mustill, S. N. Raymond, and M. B. Davies, Mon. Not. R. Astron. Soc. **460**, L109 (2016).

[89] R. J. Parker, T. Lichtenberg, and S. P. Quanz, Mon. Not. R. Astron. Soc. **472**, L75 (2017).

[90] B. V. Lehmann, O. G. Ross, A. Webber, and S. Profumo, Mon. Not. R. Astron. Soc. **505**, 1017 (2021).

[91] B. V. Lehmann, A. Webber, O. G. Ross, and S. Profumo, J. Cosmol. Astropart. Phys. 08 (2022) 079.

[92] J. Scholtz and J. Unwin, Phys. Rev. Lett. **125**, 051103 (2020).

[93] K. Mandel and E. Agol, Astrophys. J. **580**, L171 (2002).

[94] B. Carlson, Numer. Algorithms **10**, 13 (1995).

[95] M. Gillon, B.-O. Demory, A. Triaud, T. Barman, L. Hebb, J. Montalbán, P. Maxted, D. Queloz, M. Deleuil, and P. Magain, Astron. Astrophys. **506**, 359 (2009).

[96] P. Barge *et al.*, Astron. Astrophys. **482**, L17 (2008).

[97] A. Claret, Astron. Astrophys. **600**, A30 (2017).

[98] E. Gaidos and A. W. Mann, Astrophys. J. **762**, 41 (2013).

[99] F. Pereira, arXiv:2207.03019.

[100] D. Veras, in *Oxford Research Encyclopedia of Planetary Science* (Oxford University Press, New York, 2021) p. 1.